# Efficient and Goal-Directed Oscillations in Articulated Soft Robots: The Point-To-Point Case

Luigi Bono Bonacchi, Máximo A. Roa, Anna Sesselmann, Florian Loeffl, Alin Albu-Schäffer, and Cosimo Della Santina

***Abstract*—Introducing elasticity in the mechanical design can endow robots with the ability of performing efficient and effective periodic motions. Yet, devising controllers that can take advantage of such elasticity is still an open challenge. This letter tackles an instance of this general problem, by proposing a control architecture for executing goal-oriented and efficient point-to-point periodic motions. This is achieved by (i) producing motor torques that excite intrinsic modal oscillations, and simultaneously (ii) adjusting parallel elasticity so to shape the natural modes. Analytical proofs of convergence are provided for the linear approximation. The performance and efficiency (in the sense of low energy expenditure) of the method in the nonlinear case are assessed with extensive simulations and experiments.**

***Index Terms*—Compliant joints and mechanisms, motion control, natural machine motion.**

## I. Introduction

In RECENT years new types of compliant actuators have been proposed, with the aim of reducing robots' energy consumption and improving their performance. Articulated Soft Robots are the main results of this innovation [1]. Of particular relevance within this field are lockable parallel elastic actuators [2]–[4], which are especially designed for efficiency, i.e. low energy consumption for achieving the desired motion. The pre-load of springs acting in parallel to motors can be adjusted, and they are fixed without further energy expenditure by means of locks. Articulated soft robots have considerable potential for applications involving repetitive motions, e.g. pick and place [5] and locomotion [6]. Among these motions, our work focuses specifically on the efficient execution of end effector point-to-point oscillations, which covers tasks that are widespread in the practice, such as Pick-and-Place actions.

However, developing algorithms that take advantage of the elasticity in articulated soft robots is not an easy task. Classical control approaches [7]–[9] can be used when the goal is to generate precise motions. Yet, no guarantee on efficiency is embedded in these techniques. At the other end of the spectrum, we find algorithms specifically aiming at minimizing energy expenditure. For example, optimal control has been used to this end [10]–[12], with promising results that however are often limited to particular examples. More recently, a series of works by some of the co-authors [13]–[16] have proven that linear and nonlinear modal theory can be used to guide the excitation of hyper-efficient oscillations in generic soft robots. Yet, these performances are obtained at the cost of accepting whatever oscillatory behavior the system can achieve - regardless of the task's goal.

Our work proposes a control architecture that can generate *goal-oriented* oscillatory motions in articulated soft robots. More specifically, we focus here on the case of parallel actuation with adjustable lockable springs. We consider as control input the adjustable pre-loads and the joint torques - making the system strongly over-actuated (twice the actuators than the joints). Our proposed controller can exploit this large actuation space to simultaneously perform goal-directed and hyperefficient oscillations. This is done by combining a bang-bang and a repetitive controller, as concisely summarized by Fig. 1. The bang-bang controller sustains modal oscillations by compensating for damping along one eigenmode of the system, thus extending the previous work in [14]. The repetitive controller is added to induce the desired oscillation by updating the bang-bang amplitude at the end of each oscillation. We derive our analytical results using a linear approximation, which keeps the theory tractable. Afterwards, the controllers are validated in the fully nonlinear case across several conditions and tasks, including experiments and comparisons in simulations with a finely-tuned PD controller.

To sum up, we contribute to the state of the art with:

- A bang-bang controller exciting efficient modal oscillations by relying on velocity measurements;
- A repetitive controller shaping modal oscillations by adjusting mechanical parameters and a low-level gain, so to achieve two desired end goal points;
- Simulations showing that adjustable parallel elastic mechanisms can consistently reduce over 99% of the energy expenditure in point-to-point motions;
- Experiments proving the performance of the proposed strategy on a real system.

Manuscript received October 15, 2020; accepted January 31, 2021. Date of publication February 23, 2021; date of current version March 16, 2021. This letter was recommended for publication by Associate Editor B.V. Adorno and Editor A. Kheddar upon evaluation of the reviewers' comments. This work was supported by EU Projects 835284 M-Runners and 101016970 NI. *(Luigi Bono Bonacchi and Máximo A. Roa contributed equally to this work.) (Corresponding author: Maximo A. Roa.)*

Luigi Bono Bonacchi, Máximo A. Roa, Anna Sesselmann, and Florian Loeffl are with the Institute of Robotics and Mechatronics, German Aerospace Center (DLR), 82234 Wessling, Germany (e-mail: luigi.bonacchi@dlr.de; maximo.roa@dlr.de; anna.sesselmann@dlr.de; florian.loeffl@dlr.de).

Alin Albu-Schäffer is with the Institute of Robotics and Mechatronics, German Aerospace Center (DLR), 82234 Wessling, Germany, and also with the Informatics and Mathematics Department, Technical University of Munich (TUM), 85748 Munich, Germany (e-mail: Alin.Albu-Schaeffer@dlr.de).

Cosimo Della Santina is with the Institute of Robotics and Mechatronics, German Aerospace Center (DLR), 82234 Wessling, Germany, and Informatics and Mathematics Department, Technical University of Munich (TUM), 85748 Munich, Germany, and also with the Department of Cognitive Robotics, Delft University of Technology, 2628 Delft, The Netherlands (e-mail: cosimodellasantina@gmail.com).

This letter has supplementary downloadable material available at https://doi.org/10.1109/LRA.2021.3061345, provided by the authors.

Digital Object Identifier 10.1109/LRA.2021.3061345

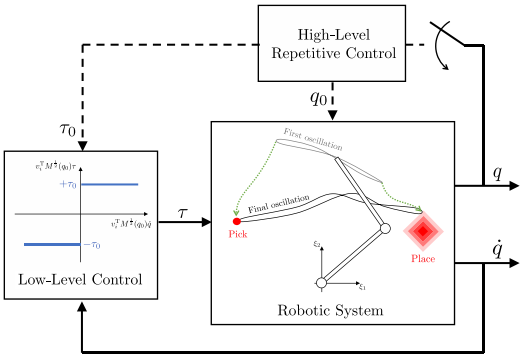


Fig. 1. Block scheme of the proposed control architecture. A low-level bang-bang controller (Eq. (6)) excites modal oscillations of an articulated soft robot by acting on the joint torques. A high-level controller (Eq. (23)) selects the low-level control amplitude $\tau_0 \in \mathbb{R}$ and the pre-loads $q_0 \in \mathbb{R}^n$ of the springs so to excite oscillations that go from a picking position to a desired placing area. The dashed lines refer to flow of information happening only at the end of each oscillation (discrete time variable $k$), while solid lines refer to continuous exchange of information (standard time $t$).

## II. Preliminaries

### A. Dynamical Model

Consider a manipulator with $n$ Degrees of Freedom (DoF). We assume that a parallel elastic mechanism with linear characteristics and adjustable pre-load is connected to each joint. We have direct control of the joint torques $\tau$ and of the pre-load $q_0$. The behaviour of this system is described by the usual second order ordinary differential equations

$$M(q)\ddot{q} + (C(q,\dot{q}) + D)\dot{q} + K(q - q_0) = \tau, \tag{1}$$

where $q \in \mathbb{R}^n$ are the joint coordinates of the robot, $\dot{q}, \ddot{q}$ are the time derivatives, $q_0 \in \mathbb{R}^n$ are the angular pre-loads given to the springs, $\tau \in \mathbb{R}^n$ are the control torques, $M(q) \in \mathbb{R}^{n\times n}$ is the inertia matrix, $C(q,\dot{q}) \in \mathbb{R}^{n\times n}$ contains the Coriolis and centrifugal terms. $D \in \mathbb{R}^{n\times n}$ and $K \in \mathbb{R}^{n\times n}$ are damping and stiffness matrices, both positive defined. Finally, we consider the forward kinematics of the robot $h : \mathbb{R}^n \to \mathbb{R}^m$ mapping the configuration of the robot $q$ into a task space $\xi = h(q)$. Without loss of generality, we consider in the following $\xi \in \mathbb{R}^m$ to be a representation of the end effector configuration.

### B. Linear Modes

Note that the equilibrium of the system for $\tau = 0$ is $q = q_0$. We can approximate (1) around said equilibrium through standard linearization, obtaining

$$M(q_0)\ddot{q} + D\dot{q} + K(q - q_0) = \tau. \tag{2}$$

For the sake of conciseness, we assume $D$ and $K$ to be simultaneously diagonalizable. The spectral analysis of the matrix $M(q_0)^{-\frac{1}{2}} K M(q_0)^{-\frac{1}{2}}$ produces the unit vectors $v_1, v_2, \ldots, v_n$ such that $\mathrm{Span}\{(v_j, 0), (0, v_j)\}$ is a (two-dimensional) eigenspace of (2). Please refer to [16] and references within for more information on modal analysis.

## III. Proposed Controller

### A. Problem Statement

Consider two configurations $q_{\mathrm{pi}}, q_{\mathrm{pl}} \in \mathbb{R}^m$. The aim of this letter is to propose a closed-loop controller which converges to a constant pre-load $q_0 \in \mathbb{R}^n$ and to a pattern of *small* joint torques $\tau \in \mathbb{R}^n$ such that the system oscillates between these two configurations. More specifically, we want that

$$\lim_{t\to\infty} ||q(t) - \bar{q}(t)|| = 0, \tag{3}$$

where $\bar{q} : \mathbb{R} \to \mathbb{R}^n$ is a periodic function of period $T > 0$ such that there exists a $t_1 > 0$ for which $\dot{\bar{q}}(t_1) = 0$ and

$$\bar{q}(t_1) = q_{\mathrm{pi}}. \tag{4}$$

Also, we ask that there exists $t_2 \in (t_1, t_1 + T)$ such that $\dot{\bar{q}}(t_2) = 0$ and

$$\bar{q}(t_2) = \arg \min_{\bar{q}\,\mathrm{s.t.}\,\bar{q}(t_1)=q_{\mathrm{pi}}} ||h(\bar{q}(t_2)) - h(q_{\mathrm{pl}})||_2^2. \tag{5}$$

We will occasionally use in the following the notation $\xi_{\mathrm{pi}} = h(q_{\mathrm{pi}})$ and $\xi_{\mathrm{pl}} = h(q_{\mathrm{pl}})$. We formulate (5) in this way - rather than as a copy of (4) - to enforce a priority hierarchy between the two tasks. This is necessary because it may not be possible to achieve the two conditions simultaneously, for reasons that will become clear later. This is consistent with an interpretation of the problem as a periodic pick-and-place task. Indeed, to pick an object we should be very precise, while often there is more freedom in terms of where we can place the object.

### B. Problem Solution in Brief

Two sub-goals can be recognized in the above problem statement: (i) reliably sustaining (efficient) oscillations as required by (3), and (ii) adjusting these oscillations so to verify (4) and (5). These two sub-goals are addressed by a low-level and a high-level controller respectively, as summarized in Fig. 1.

The low-level controller (Section IV) achieves its goal by producing a bang-bang excitation in the direction of a system's eigenvector $v_i$. By acting in the direction of the mode we do not combat the natural dynamics of the robot [15], and we only act against the dissipation. Physical dissipation acts as a stabilizing force, damping the oscillation happening in the direction of $v_{j\neq i}$. The control parameters that are left to be selected by the high-level controller (Section V) are the overall amplitude of the bang-bang excitation $\tau_0 \in \mathbb{R}$ and the pre-loads $q_0 \in \mathbb{R}^n$. Intuitively, they correlate with amplitude and direction of the natural oscillation, respectively. The controller observes the oscillation generated by the low-level bang-bang and iteratively adjusts these $n + 1$ parameters in a piece-wise constant fashion, so to steer the mechanical system towards presenting natural evolutions that verify the sub-goal (ii).

The proposed control architecture is derived by focusing on the linear case (2). This is necessary to keep the theory tractable. Consider for example that nonlinear modes for robotic systems are defined only for conservative systems [16]. We will focus on the nonlinear case in future work. More importantly, thanks to their feedback nature, the resulting controllers work well in the practice when applied to the full-fledged nonlinear system (1), as discussed in Sections VI and VII.

## IV. Low-Level Bang-Bang Excitation

We want to compensate for damping in the direction of a system's eigenvector $v_i$, while suppressing all the oscillations happening in the orthogonal direction $v_{j\neq i}$. Indeed, a system as (2) naturally and autonomously oscillates in the direction of $v_i$, whenever dissipative forces are null in that direction [16]. Perfect compensation of dissipation would require $\tau = D\dot{q}$. Yet, perfectly estimating the damping contributions is unfeasible in practice. As an alternative, we consider the following bang-bang excitation that generates a stable limit cycle for a vast range of control gains

$$\tau = \tau_0 M^{\frac{1}{2}}(q_0) v_i \text{sign}\Big(v_i^{\mathrm{T}} M^{\frac{1}{2}}(q_0)\dot{q}\Big), \tag{6}$$

where $v_i$ is the $i-$th eigenvector of $M^{-\frac{1}{2}}(q_0)KM^{-\frac{1}{2}}(q_0)$ and $M^{-\frac{1}{2}}(q_0)DM^{-\frac{1}{2}}(q_0)$, with associated eigenvalues $\tilde{d}_i$ and $\tilde{k}_i$. $\tau_0 \in \mathbb{R}$ is any positive gain.

*Lemma 1:* The closed loop (2), (6) admits as solution a periodic evolution $\tilde{q}$ of period $T$, if $\exists T \neq 0$ such that

$$\Big[(e^{A_i T} - I)^{-1}(e^{A_i \frac{T}{2}} - I)^2 A_i^{-1}\Big]_{2,2} = 0, \tag{7}$$

where $[\cdot]_{2,2}$ extracts the element in position (2,2) of the argument, and

$$A_i = \begin{bmatrix} 0 & 1 \\ -\tilde{k}_i & -\tilde{d}_i \end{bmatrix}. \tag{8}$$

Furthermore, the steady state evolution $\tilde{q}$ is such that

$$v_j^{\mathrm{T}} M^{\frac{1}{2}}(\tilde{q} - q_0) = 0, \quad \forall j \neq i. \tag{9}$$

*Proof:* We introduce the change of coordinates

$$q = M^{-\frac{1}{2}} V \psi, \quad \dot{q} = M^{-\frac{1}{2}} V \dot{\psi}, \tag{10}$$

where $V \in \mathbb{R}^{n\times n}$ is the unit matrix having as $j-$th column $v_j$. Then (2) can be re-written as

$$\ddot{\psi} + \tilde{D}\dot{\psi} + \tilde{K}(\psi - \psi_0) = V^{\mathrm{T}} M^{-\frac{1}{2}} \tau \tag{11}$$

where we pre-multiplied by $V^{\mathrm{T}} M^{-\frac{1}{2}}$. We also defined $q_0 = M^{-\frac{1}{2}} V \psi_0$, $\tilde{D} = V^{\mathrm{T}} M^{-\frac{1}{2}} D M^{-\frac{1}{2}} V$ and $\tilde{K} = V^{\mathrm{T}} M^{-\frac{1}{2}} K M^{-\frac{1}{2}} V$ - the latter two being diagonal matrices by definition. Thus, introducing (6) yields

$$\ddot{\psi} + \tilde{D}\dot{\psi} + \tilde{K}(\psi - \psi_0) = \tau_0 [0 \dots 0\, 1\, 0 \dots 0]^{\mathrm{T}} \text{sign}(\dot{\psi}_i), \tag{12}$$

where we exploited that $V^{\mathrm{T}} V = I$, and we defined $\dot{\psi}_i$ as $i-$th element of $\dot{\psi}$. Since all matrices involved are diagonal, (12) is equivalent to $n$ decoupled equations. More specifically, for all $j \neq i$ we have

$$\ddot{\psi}_j + \tilde{d}_j \dot{\psi}_j + \tilde{k}_j(\psi_j - \psi_{0,j}) = 0 \tag{13}$$

with $\tilde{d}_j$, $\tilde{k}_j$ being the $j-$th diagonal element of $\tilde{D}$, $\tilde{K}$, and $\psi_j$, $\psi_{0,j}$ the $i-$th element of $\psi$, $\psi_0$. Eq. (13) is a damped oscillator with strictly positive impedance by hypothesis. Therefore,

$$\lim_{t\to\infty} \psi_j = \psi_{0,j} \Rightarrow \lim_{t\to\infty} v_j^{\mathrm{T}} M^{\frac{1}{2}} q = v_j^{\mathrm{T}} M^{\frac{1}{2}} q_0, \tag{14}$$

where we used (11). This proves (9). Now, we need to prove that the steady state evolution is periodic and non constant. This is equivalent to show that $\psi_i(t)$ has the same characteristics. Its dynamics is

$$\ddot{\psi}_i + \tilde{d}_i \dot{\psi}_i + \tilde{k}_i(\psi_i - \psi_{0,i}) = \tau_0 \text{sign}(\dot{\psi}_i). \tag{15}$$

To see if this equation admits a periodic solution $\tilde{q}$, we consider the return map $\psi_i(t) \to \psi_i(t+T)$, with $T \in \mathbb{R}$ being the unknown period of the oscillation. We then search for its fixed points. This is equivalent to imposing the periodicity condition

$$\psi_i(0) = \psi_i(T). \tag{16}$$

Among all possible solutions, we search for a symmetrical one, i.e. that $\dot{\psi}_i$ switches sign only once within a cycle at half of the period, i.e. $\dot{\psi}_i(0) = \dot{\psi}_i(T/2) = 0, \dot{\psi}_i(t) > 0$ if $t \in (0, T/2)$, and $\dot{\psi}_i(T/2) < 0$ if $t \in (T/2, T)$. We took $t = 0$ without loss of generality. We now integrate (15) for half a period, obtaining

$$\begin{bmatrix} \psi_i(\frac{T}{2}) - \psi_{0,i} \\ 0 \end{bmatrix} = e^{A_i \frac{T}{2}} \begin{bmatrix} \psi_i(0) - \psi_{0,i} \\ 0 \end{bmatrix} + (e^{A_i \frac{T}{2}} - I) A_i^{-1} \begin{bmatrix} 0 \\ \tau_0 \end{bmatrix}. \tag{17}$$

Integrating for a further $T/2$ similarly yields

$$\begin{bmatrix} \psi_i(T) - \psi_{0,i} \\ 0 \end{bmatrix} = e^{A_i \frac{T}{2}} \begin{bmatrix} \psi_i(\frac{T}{2}) - \psi_{0,i} \\ 0 \end{bmatrix} - (e^{A_i \frac{T}{2}} - I) A_i^{-1} \begin{bmatrix} 0 \\ \tau_0 \end{bmatrix}. \tag{18}$$

We combine now (16), (17), and (18). The result is

$$\begin{bmatrix} \psi_i(0) - \psi_{0,i} \\ 0 \end{bmatrix} = (e^{A_i T} - I)^{-1}(e^{A_i \frac{T}{2}} - I)^2 A_i^{-1} \begin{bmatrix} 0 \\ \tau_0 \end{bmatrix}. \tag{19}$$

These are two equations that need to be simultaneously fulfilled. Hypothesis (7) assures that a $T$ exists, verifying the second equation. Note that the same condition results from integrating twice starting from $T/2$. The first equation of (19) is then always solved by selecting the opportune $\psi_i(0)$. ■

Note that we are not writing the explicit form of the final oscillation just for the sake of space. This can be obtained by forward integrating the dynamics starting from (19) and in the same fashion of (17) when $t \in (wT, (w+1/2)T)$, and of (18) when $t \in ((w+1/2)T, (w+1)T)$, for any $w \in \mathbb{Z}$.

*Corollary 1:* If the hypotheses of Lemma 1 are verified, then the equilibrium oscillation $\tilde{q}$ is expression of a limit cycle (i.e. locally stable) if

$$|e^{-\frac{T}{4}} e^{\tilde{d}\left(1 \pm \sqrt{1 - 4\frac{\tilde{k}}{\tilde{d}^2}}\right)}| < 1. \tag{20}$$

*Proof:* First consider that for any two square real matrices $E_1$ and $E_2$, the following holds $\rho(E_1 E_2) < \rho(E_1)\rho(E_2)$, where $\rho(\cdot)$ is the spectral radius. Furthermore, if $\lambda_i$ is an eigenvalue of $E_1$, then $e^{\lambda_i}$ is an eigenvalue of $e^{E_1}$. Combining these two properties with [17, Theorem 3.1] and (15) trivially yields (20). ■

It is interesting to point out that neither (7) nor (20) depend on $\tau_0$. Therefore, if a limit cycle exists for some $\tau_0$, it will exist with the same frequency for all possible amplitudes of the bang-bang. The resulting evolution will be nonetheless different. More specifically, the amplitude will linearly increase with $\tau_0$.

We conclude this section by remarking that the use of nonlinear algebraic feedbacks to put dynamical systems in oscillation

is well known in identification theory [17]. Yet, their use in purposeful excitation of oscillations in mechanical systems is a rather new area. [14] proposed a bang-bang action for non-linear mechanical systems with one DoF. That controller is position-based and therefore not tailored for producing efficient oscillations. More recently, we preliminary investigated the use of a velocity-based bang-bang action in [18]. That controller is tailored to a very specific example and no general theoretical analysis is provided. Yet, the good experimental performance observed in that work motivated us towards developing the general controller (6) that we have proposed in this section.

## V. High-Level Repetitive Controller

Eqs. (17) and (18) relate - through (10) - the ends of the oscillation to the the $n+1$ parameters $\tau_0 \in \mathbb{R}$ and $q_0 \in \mathbb{R}^n$. Note that the low-level controller already fixes $n-1$ of the $n$ degrees of actuation in $\tau$, by always pointing in the direction of the selected eigenvector $v_i$. It also defines the time evolution of $\tau$. Only the overall amplitude $\tau_0$ is left free to be selected. In this section we propose a discrete controller that iteratively updates these inputs to move the oscillations towards the desired target locations.

Combining (10) and (19) together with the first equations of (17) and (18) leads to the following set of algebraic equations (which we do not write explicitly for the sake of space)

$$\begin{bmatrix} q_{\mathrm{pi}} \\ q_{\mathrm{pl}} \end{bmatrix} = P(q_0) \begin{bmatrix} q_0 \\ \tau_0 \end{bmatrix}, \tag{21}$$

where $P \in \mathbb{R}^{2n\times(n+1)}$ is the matrix that results by collecting the other terms.

Then, we introduce the time-discrete variable $k \in \mathbb{Z}$. At each step $k$ we allow ourselves to change $q_0^k$ and $\tau_0^k$. As a consequence, according to Lemma 1, the system will reach a steady state $q_{\mathrm{pi}}^k$ and $q_{\mathrm{pl}}^k$. After the steady state oscillation is reached, we move to step $k+1$, and so on. The result is

$$\begin{bmatrix} q_{\mathrm{pi}}^k \\ q_{\mathrm{pl}}^k \end{bmatrix} = \begin{bmatrix} \tilde{P}(q_0^k) \\ C(q_0^k) \end{bmatrix} \begin{bmatrix} q_0^k \\ \tau_0^k \end{bmatrix} \tag{22}$$

where we also partitioned $P$ in its top block $\tilde{P} \in \mathbb{R}^{(n+1)\times(n+1)}$ and in its bottom part $C \in \mathbb{R}^{(n-1)\times(n+1)}$. In this way, we artificially introduce a further time dimension that we can use to close the following control loop

$$\begin{bmatrix} q_0^{k+1} \\ \tau_0^{k+1} \end{bmatrix} = \begin{bmatrix} q_0^k \\ \tau_0^k \end{bmatrix} + \tilde{P}^{\dagger}(q_0^k) \begin{bmatrix} \bar{q}_{\mathrm{pi}} - q_{\mathrm{pi}}^k \\ -\frac{[1\ r(q_0^k)]}{1+||r(q_0^k)||_2^2} \nabla F(q_{\mathrm{pl}}^k) \end{bmatrix}, \tag{23}$$

where $r(q_0^k) = [0 \dots 0\ 1]\tilde{P}^{\dagger\mathrm{T}} C^{\mathrm{T}}$, $F(q_{\mathrm{pl}}) = ||h(\bar{q}_{\mathrm{pl}}) - h(q_{\mathrm{pl}})||_2^2$, and $P^{\dagger}$ is the Moore-Penrose pseudo-inverse of $P$. This way of specifying the preset $q_0$ inherently leads to a piecewise constant evolution, as imposed by the problem statement.

*Lemma 2:* The closed loop (22), (23) is such that

$$\lim_{k\to\infty} q_{\mathrm{pi}}^k = \bar{q}_{\mathrm{pi}}, \tag{24}$$

and $q_{\mathrm{pl}}^k$ evolves so to move at each step as close as possible to the direction of maximum decrease of $F$ - i.e. so to greedily verify (5) - if $\det(\tilde{P}) \neq 0$.

*Proof:* We pre-multiply (23) by $P(q_0)$, and we combine it with (21), obtaining

$$\begin{bmatrix} q_{\mathrm{pi}}^{k+1} \\ q_{\mathrm{pl}}^{k+1} \end{bmatrix} = \begin{bmatrix} q_{\mathrm{pi}}^k \\ q_{\mathrm{pl}}^k \end{bmatrix} + P\tilde{P}^{\dagger} \begin{bmatrix} \bar{q}_{\mathrm{pi}} - q_{\mathrm{pi}}^k \\ -\frac{[1\ r(q_0^k)]}{1+||r(q_0^k)||_2^2} \nabla F(q_{\mathrm{pl}}^k) \end{bmatrix}, \tag{25}$$

If $\det(P) \neq 0$ then $\tilde{P}^{\dagger} = \tilde{P}^{-1}$. Thus (25) becomes

$$\begin{bmatrix} q_{\mathrm{pi}}^{k+1} \\ q_{\mathrm{pl}}^{k+1} \end{bmatrix} = \begin{bmatrix} q_{\mathrm{pi}}^k \\ q_{\mathrm{pl}}^k \end{bmatrix} + \begin{bmatrix} I \\ C\tilde{P}^{-1} \end{bmatrix} \begin{bmatrix} \bar{q}_{\mathrm{pi}} - q_{\mathrm{pi}}^k \\ -\frac{[1\ r(q_0^k)]}{1+||r(q_0^k)||_2^2} \nabla F(q_{\mathrm{pl}}^k) \end{bmatrix}, \tag{26}$$

where $I \in \mathbb{R}^{(n+1)\times(n+1)}$ is the identity matrix.

The first set of $n$ equations becomes $q_{\mathrm{pi}}^{k+1} = \bar{q}_{\mathrm{pi}}$. Thus, that end of the oscillation converges in one step from $q_{\mathrm{pi}}^k$ to the desired value $\bar{q}_{\mathrm{pi}}$. We focus now on the second set of equations, which after one step becomes

$$q_{\mathrm{pl}}^{k+1} = q_{\mathrm{pl}}^k + \begin{bmatrix} 0 \dots 0\ 1 \\ \tilde{P}^{-1}C \end{bmatrix} \begin{bmatrix} 0 \\ -\frac{[1\ r(q_0^k)]}{1+||r(q_0^k)||_2^2} \nabla F(q_{\mathrm{pl}}^k) \end{bmatrix}. \tag{27}$$

Simple algebraic manipulations produce

$$q_{\mathrm{pl}}^{k+1} = q_{\mathrm{pl}}^k - \begin{bmatrix} 1 \\ r^{\mathrm{T}}(q_0^k) \end{bmatrix} \frac{[1\ r(q_0^k)]}{1+||r(q_0^k)||_2^2} \nabla F(q_{\mathrm{pl}}^k). \tag{28}$$

Which is a projected gradient descent. Note indeed that $[1\ r]/(1+||r||_2^2)$ is the Moore-Penrose pseudo-inverse of the vector $[1\ r]^{\mathrm{T}}$. This algorithm selects among all the changes of $q_{\mathrm{pl}}^k$ compatible with the primary task (4), the one which is closest to the direction of steepest decreasing of $F$ (i.e. $-\nabla F(q_{\mathrm{pi}}^k)$), therefore eventually fulfilling (5). ■

To conclude, it is important to stress that the condition $\det(\tilde{P}(q_0^k)) \neq 0$ is quite hard to check a priori, since it is control-dependent. Yet, our numerical analyses show that this condition is always verified for all configurations of all the robots tested. Future work will be devoted to analytically prove the universality of this property.

## VI. Simulations

### A. Low-Level Controller

To showcase the performance of (6) when dealing with full-fledged nonlinear systems, we consider the excitation of nonlinear oscillations in a 4-DoF serial robot with revolute joints. The robot has uniformly distributed masses, and each link is 4 kg. The first two links are 0.3 m long, the remaining two are 0.15 m long. The impedance is $K = 5I$ Nmrad$^{-1}$ and $D = 0.05I$ Nmsrad$^{-1}$, with $I$ being the identity matrix. We excite the system towards the eigenvector

$$M^{-\frac{1}{2}} v_i \simeq (-0.86, -0.48, -0.16, -0.04). \tag{29}$$

This corresponds to a coordinated swing motion of the four links. Both conditions (7) and (20) are verified by a period $T$ equal up to the second significant digit to the natural frequency of oscillation of the system. This speaks for the ability of the proposed bang-bang controller to excite natural oscillations. This ability will be later quantified by looking at the efficiency.

Fig. 2 shows one cycle of the obtained oscillations for all joints. The bang-bang controller correctly switches along with the angular velocities, always injecting energy in the opposite direction of the dissipation. The resulting motions are in phase.

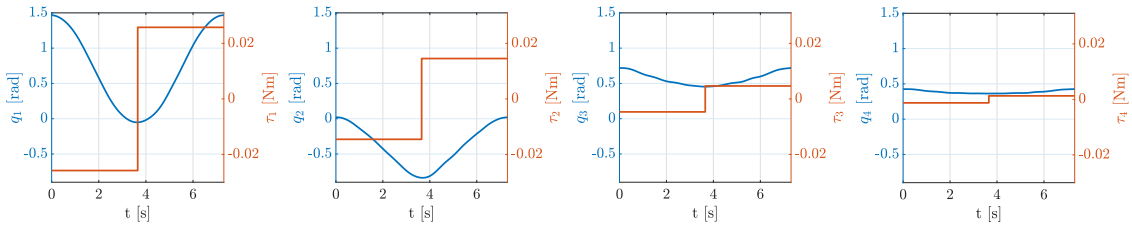


Fig. 2. A single steady-state oscillation obtained in simulation with a 4-DoF serial robot, when excited with the proposed bang-bang controller. We excite the system in the direction of (29) with gain $\tau_0 = 0.25$ Nm.

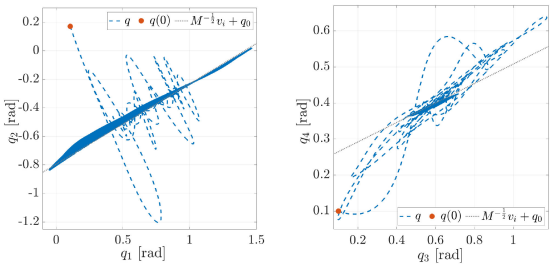


Fig. 3. Configuration space trajectories obtained in simulation with a 4-DoF serial manipulator, when excited with the proposed bang-bang controller. Despite being a highly nonlinear system, the trajectories nicely converge towards the nominal eigenvector. Note that the steady state oscillations of $q_3$ and $q_4$ are small, and well aligned to the mode - not to be confused with the large transient.

They are also closely aligned to the desired eigenvector, as shown by Fig. 3.

### *B. Comparison With a PD Controller*

The aim of this subsection is to extensively test the full controller (6) (23), across several initial conditions, against a state-of-the-art controller, and on three different robotic systems. The considered robotic systems include the 4-DoF robot used in the previous subsection, together with a 2-DoF and a 3-DoF serial manipulators. These two robots have links of the same length and same mass, which sum up to the same total mass and length of the 4-DoF robot. As state-of-the-art comparison we consider a PD controller with steady state compensation of the potential field

$$\tau = \kappa(\bar{q} - q) - \beta\dot{q} + K(\bar{q} - q_0). \tag{30}$$

We select the reference $\bar{q}$ as a square wave with the same period of the natural oscillation of the robot, and alternating between $\bar{q}_{\mathrm{pi}}$ and $\bar{q}_{\mathrm{pl}}$. The control gains are $\kappa, \beta \in \mathbb{R}$, with $\beta = 2\sqrt{\kappa}$. We tune $\kappa$ so to achieve precise convergence in $T/2$. $K$ is the exact stiffness as in (1). The initial pre-loads are set to $q_0 = 0$.

We ran a Monte Carlo comparison with 360 tests (120 per robot). For both controllers, the system performs a periodic point-to-point motion between target locations that are randomly extracted from two Gaussian distributions. The mean values are respectively the centroid of the working-space's first and fourth quadrants. The variance $\sigma$ is selected so that the circle with radius $3\sigma$ is the biggest one fully included in the workspace.

The results of this analysis are shown in Fig. 4. The finely-tuned PD and the proposed control architecture have comparable performance in terms of precision. The latter is better in reaching the pick location and the former in getting to the place location. Fig. 5 shows an example of evolution of the end effector position

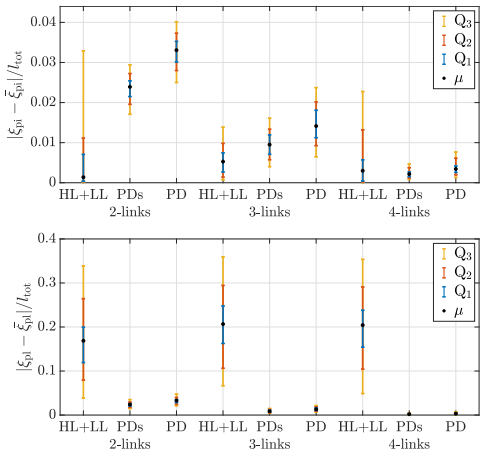


Fig. 4. Monte Carlo simulations (360 tests) comparing the proposed controller (HL+LL) pick-and-place precision against a finely tuned PD - with (PDs) and without (PD) springs. We report average performance $\mu$, together with quartiles.
.

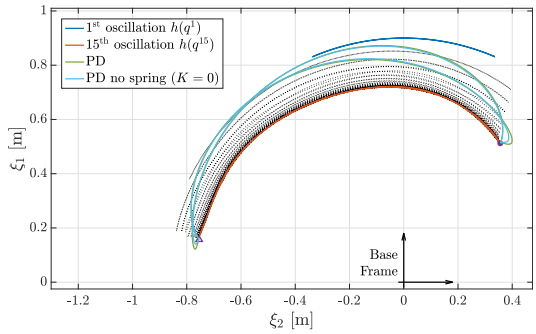


Fig. 5. End effector trajectories obtained in simulation with a 4-DoF serial manipulator, when controlled with a finely-tuned PD or with the proposed architecture. The gray dotted lines are the oscillations from $2^{\mathrm{nd}}$ to $14^{\mathrm{th}}$ iterations of the proposed high-level controller. The goal locations $h(\bar{q}_{\mathrm{pi}})$ and $h(\bar{q}_{\mathrm{pl}})$ are depicted with a purple dot and a triangle, respectively.

$\xi$ in Cartesian coordinates. The first and last oscillations are highlighted in blue and orange, respectively. The intermediate oscillations are shown with black dotted lines. The evolution produced by the PD controller is also shown, in light blue. Fig. 6 shows the evolution of pick errors and the cost function. Both go to zero, and convergence happens within a small number of steps.

We measure the control effort (i.e. efficiency) by integrating the power required to sustain an oscillation at steady state $\int_0^T \dot{q}^{\mathrm{T}}\tau$, where $T \in \mathbb{R}$ is the period of oscillation. Fig. 7 shows

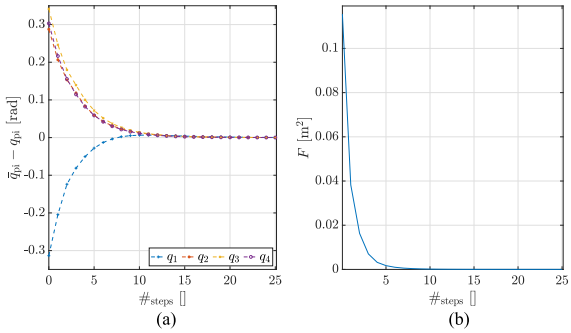


Fig. 6. Evolution of error for the picking configuration (a), and the cost function (b) at each step, when the complete control architecture is applied to a serial robot with four links.

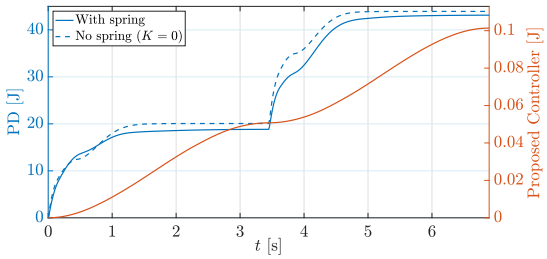


Fig. 7. Example of time evolution of the energy expenditure required to sustain the desired oscillation with the PD controller (blue) and the proposed controller (orange). Note that the two differ by two degrees of magnitude.

TABLE I
PHYSICAL PARAMETERS OF THE PANTOGRAPH ARM. THE CENTER OF MASS LOCATION IS EXPRESSED W.R.T. THE PREVIOUS JOINT

| | Mass [g] | Inertia [kg mm$^2$] | Length [mm] | CoM [mm] |
|---|---|---|---|---|
| Link 1 | 207 | 446 | 64 | 10 |
| Link 2 | 126 | 140 | 133 | 67 |
| Link 3 | 30 | 70 | 133 | 10 |
| Link 4 | / | / | 133 | / |
| Tip mass | 0-109 | / | / | / |

an example of the time evolution of the energy expenditure for the final cycle of the example discussed above. Note that we had to use two different scales for the two evolutions, since the energy consumption is two degrees of magnitude higher for the PD. Among the 360 simulations, the proposed control architecture consistently achieves more than 99% of reduction with respect to the PD controller for all 2, 3, and 4-link robots. Interestingly, removing springs ($K = 0$) reduces the performance of the PD controller in less than 2%. This suggests that having springs is not beneficial if they are not properly and explicitly exploited by the controller.

## VII. EXPERIMENTAL EVALUATION

### A. Experimental Setup

We consider a 2-DoF arm with a parallel pantograph mechanism (4 links, 2 DoF), which is shown in Fig. 8. The arm is designed to have an interchangeable tip, so that the mass at the end effector can be adjusted. We performed experiments with and without an extra tip mass. Table I summarizes the physical parameters for the arm. The identified stiffness and damping

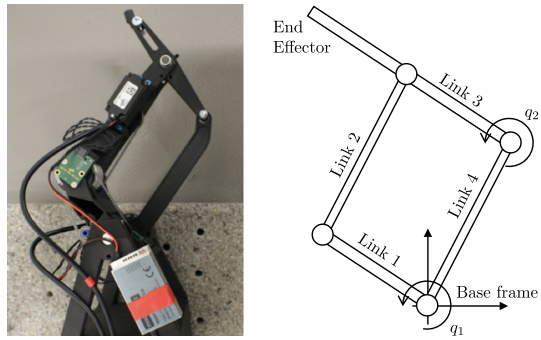


Fig. 8. The experimental setup used to test our control architecture, together with a schematic representation highlighting its main components. This is a pantographic arm, with four links but two DoF (parallel mechanism). The arm base is screwed on a block to offer a fixed base for the motion.

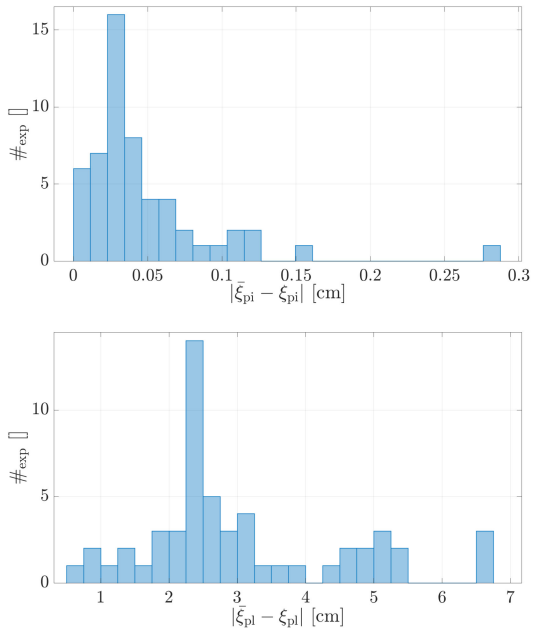


Fig. 9. Histograms of experimental performance resulting from 56 experiments. Precision is measured in reaching the two desired locations with the end effector.

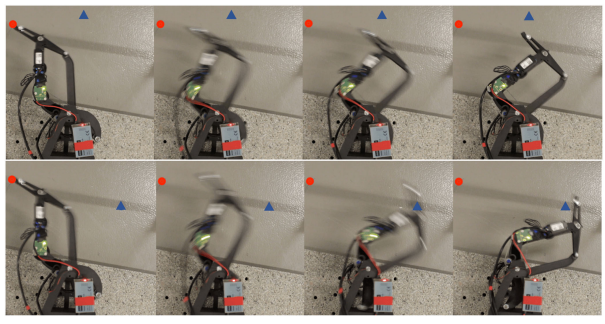

Fig. 10. Snapshots of two oscillations (top and bottom rows) of the experimental system during the first set of experiments, where only the place location $\bar{q}_{pl}$ is changed. Pick and place locations are highlighted with red dots and blue triangles, respectively. In these pictures, no mass is attached to the tip of the robot.

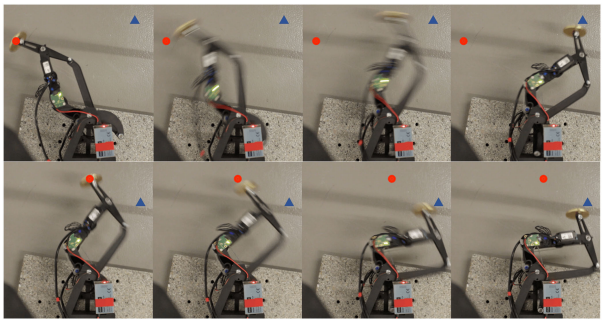

Fig. 11. Snapshots of two oscillations (top and bottom rows) of the experimental system during the second set of experiments, where the pick ($\bar{q}_{\mathrm{pi}}$) and place ($\bar{q}_{\mathrm{pl}}$) locations are changed. Pick and place locations are highlighted with red dots and blue triangles, respectively. In these pictures, the 109 g mass is attached to the tip of the robot.

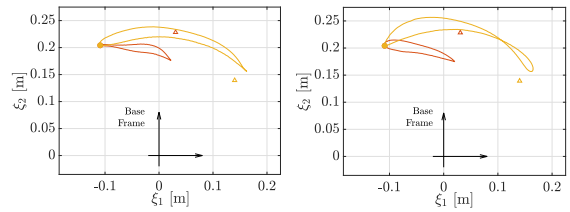


(a) Experiment 1, no extra mass (b) Experiment 1, 109g

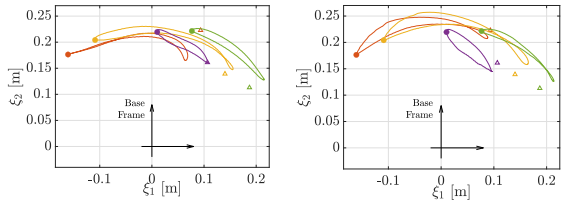


(c) Experiment 2, no extra mass (d) Experiment 2, 109g

Fig. 12. End effector trajectories at the final limit cycle for two sets of experiments making 12 of the total 56 experiments performed. Different colors represent different experiments. Tests are repeated with and without tip mass, with comparable results. The desired pick and place locations are shown with dots and triangles of the same colors. (a) Experiment 1, no extra mass. (b) Experiment 1, 109g. (c) Experiment 2, no extra mass. (d) Experiment 2, 109g.

are $k = 1.75\mathrm{Nmrad}^{-1}$ and $d = 0.03\mathrm{Nmsrad}^{-1}$, respectively. The system is actuated through two serial elastic actuators acting at the joints connecting the base to link 1, and link 1 to link 2. The angular velocities are obtained from joint positions through differentiation. We select as target eigenvalue the one associated to swing oscillations with the two links moving in phase. Conditions of Lemma 1 and Corollary 1 are verified for all the conditions tested. We take as initial high-level control action $\tau_0^0 = 1\mathrm{Nm}$ and $q_0^0 = [-0.7\ 1.1]^T$ rad.

### B. Experiments

We tested the proposed control architecture in 56 point-to-point motions, equally split in with and without tip mass. Every time, we let the system stabilize, and then changed $q_{\mathrm{pi}}$ and $q_{\mathrm{pl}}$ so to uniformly cover the whole operative space of the robot. We achieved an average error for the picking location of 0.0473 cm and of 3.43 cm for the placing location. The full distribution of the experimental errors is shown in Fig. 9. Note that the results are coherent with the ones achieved in simulation. Direct

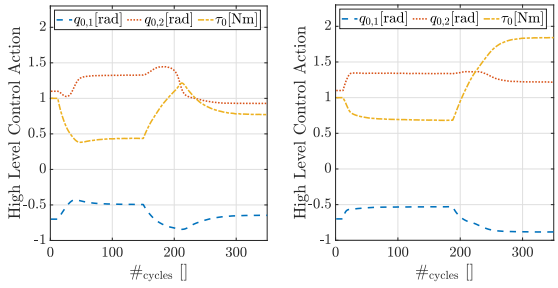


(a) No tip mass (b) 109g

Fig. 13. Evolution of the pre-loads $q_0$ and the overall control amplitude $\tau_0$, as specified by the high-level controller during the first set of experiments. (a) No tip mass. (b) 109g.

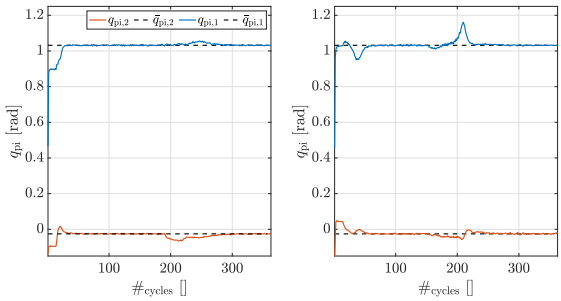


Fig. 14. Evolution of the two ends of the oscillations excited by the low-level controller $q_{\mathrm{pi}} = q^k(0)$ and $q_{\mathrm{pl}} = q^k(T/2)$, as resulting from the action of the high-level controller during the first set of experiments.

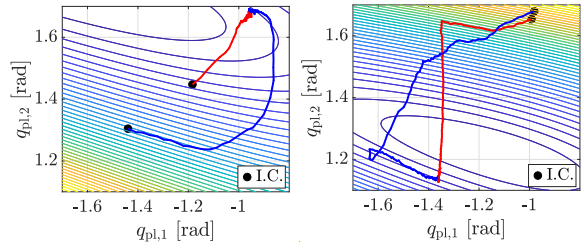


(a) First placing target (b) Second placing target

Fig. 15. Evolution of the placing location $q_{\mathrm{pl}}^k$ as result of the action of the full architecture, for the first set of experiments. This is superimposed with the isolines of $F$. The initial condition (I.C.) of the system is indicated with a solid circle. Both results with and without tip mass are reported - blue and red lines respectively. (a) First placing target. (b) Second placing target.

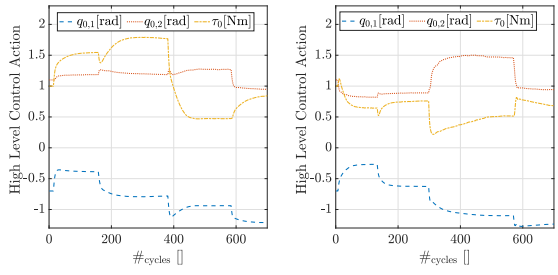


(a) No tip mass (b) 109g

Fig. 16. Evolution of the pre-loads $q_0$ and the overall control amplitude $\tau_0$, as specified by the high-level controller during the second set of experiments. (a) No tip mass. (b) 109g.

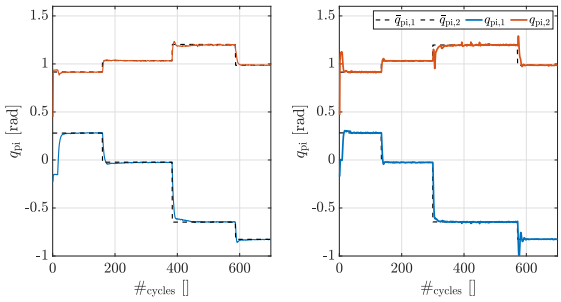


(a) No tip mass (b) 109g

Fig. 17. Evolution of the two ends of the oscillations excited by the low-level controller $q_{\text{pi}} = q^k(0)$ and $q_{\text{pl}} = q^k(T/2)$, as resulting from the action of the high-level controller during the second set of experiments. (a) No tip mass. (b) 109g.

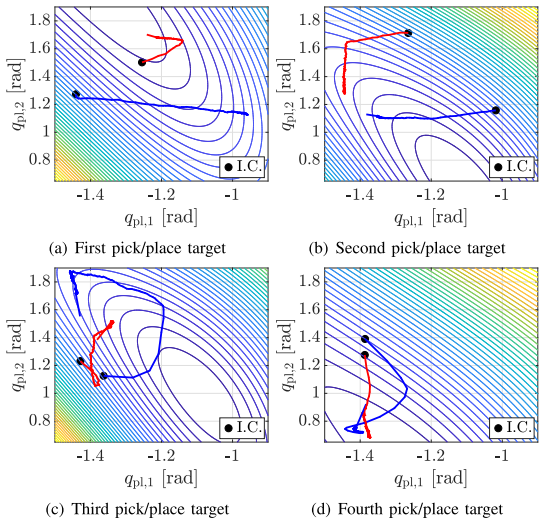


(a) First pick/place target (b) Second pick/place target

(c) Third pick/place target (d) Fourth pick/place target

Fig. 18. Evolution of the placing location $q^k_{\text{pl}}$ as result of the action of the full architecture, for the second set of experiments. This is superimposed with the isolines of $F$. The initial condition (I.C.) of the system is indicated with a solid circle. Both results with and without tip mass are reported - blue and red lines respectively. (a) First pick/place target. (b) Second pick/place target. (c) Third pick/place target. (d) Fourth pick/place target.

measurement of energy consumption was not possible due to technological limits.

Among the 56 experiments, we will focus on 12 representative ones, which we divide in two sets. Two examples of oscillations from the first set of experiments are shown in Fig. 10. We test the ability of the controller for switching from one $h(\bar{q}_{\text{pl}})$ to another, while keeping $h(\bar{q}_{\text{pi}})$ fixed. Figs. 12(a,b) report the steady state end effector trajectories, with and without tip mass, respectively. Fig. 13 shows the evolution of the high-level control inputs. For both system configurations, the pick position is correctly kept, with just small variations during the switch of desired place. This can be clearly seen from Fig. 14. Fig. 15 shows the evolution of the place position, both systems evolve correctly along the level curves of $F$ - eventually minimizing it locally.

We also report a second set of experiments, made with four consecutive choices of different pick and place locations, repeated with and without tip mass. Fig. 11 shows two examples of final oscillations, obtained with the larger tip mass. Figs. 12(c,d) show the four limit cycles. Fig. 16 depicts the control actions generated by the high-level controller. The convergence is smooth for both the pick (Fig. 17) and place (Fig. 18), resulting in a consistent decreasing of $F$.

## VIII. Conclusion and Future Work

This work proposed a new control architecture to excite and shape goal-oriented modal oscillations of an articulated soft robot. The validation showed promising performances in terms of efficiency and precision. Future work will be devoted to increasing place precision, by either further increasing the actuation space - e.g. variable stiffness mechanisms - or by focusing on task space oscillations. The robustness of the obtained oscillations will also be considered. We will also speed up the convergence process of the high-level controller by explicitly taking into account nonlinear effects.

## References


[1] C. Della Santina, M. G. Catalano, and A. Bicchi, "Soft robots," *Encyclopedia of Robotics*, M. Ang, O. Khatib, and B. Siciliano, Eds. Berlin, Germany: Springer, 2020.

[2] M. Plooij, G. Mathijssen, P. Cherelle, D. Lefeber, and B. Vanderborght, "Lock your robot: A. review of locking devices in robotics," *IEEE Robot. Automat. Mag.*, vol. 22, no. 1, pp. 106–117, Mar. 2015.

[3] G. Mathijssen *et al.*, "Novel lockable and stackable compliant actuation unit for modular SPEA actuators," *IEEE Robot. Automat. Lett.*, vol. 4, no. 4, pp. 4445–4451, Oct. 2019.

[4] M. Plooij, M. Wisse, and H. Vallery, "Reducing the energy consumption of robots using the bidirectional clutched parallel elastic actuator," *IEEE Trans. Robot.*, vol. 32, no. 6, pp. 1512–1523, Dec. 2016.

[5] F. Angelini, C. Petrocelli, M. G. Catalano, M. Garabini, G. Grioli, and A. Bicchi, "SoftHandler: An integrated soft robotic system for the handling of heterogeneous objects," *IEEE Robot. Automat. Mag.*, vol. 27, no. 3, pp. 55–72, Sep. 2020.

[6] Z. Gan, Y. Yesilevskiy, P. Zaytsev, and C. D. Remy, "All common bipedal gaits emerge from a single passive model," *J. Roy. Soc. Interface*, vol. 15, no. 146, 2018, Art no. 20180455.

[7] M. W. Spong, "Adaptive control of flexible joint manipulators," *Syst. Control Lett.*, vol. 13, no. 1, pp. 15–21, 1989.

[8] A. De Luca, B. Siciliano, and L. Zollo, "PD control with on-line gravity compensation for robots with elastic joints: Theory and experiments," *Automatica*, vol. 41, no. 10, pp. 1809–1819, 2005.

[9] M. Keppler, D. Lakatos, C. Ott, and A. Albu-Schäffer, "Elastic structure preserving (ESP) control for compliantly actuated robots," *IEEE Trans. Robot.*, vol. 34, no. 2, pp. 317–335, Apr. 2018.

[10] D. Braun, M. Howard, and S. Vijayakumar, "Optimal variable stiffness control: Formulation and application to explosive movement tasks," *Auton. Robots*, vol. 33, no. 3, pp. 237–253, 2012.

[11] G. Carabin, I. Palomba, E. Wehrle, and R. Vidoni, "Energy expenditure minimization for a Delta-2 robot through a mixed approach," *Multibody Dynamics*. A. Kecskemethy and F. Geu, Eds. Berlin, Germany: Springer, 2020, vol. 53, pp. 383–390.

[12] T. Marcucci, M. Garabini, G. Gasparri, A. Artoni, M. Gabiccini, and A. Bicchi, "Parametric trajectory libraries for online motion planning with application to soft robots," *Robotics Research*. Berlin, Germany: Springer, 2019, vol. 10, pp. 1001–1017.

[13] D. Lakatos, M. Görner, F. Petit, A. Dietrich, and A. Albu-Schäffer, "A modally adaptive control for multi-contact cyclic motions in compliantly actuated robotic systems," in *Proc. IEEE/RSJ Int. Conf. Intell. Robots Syst.*, 2013, pp. 5388–5395.

[14] D. Lakatos and A. Albu-Schäffer, "Switching based limit cycle control for compliantly actuated second-order systems," in *Proc. IFAC World Congr.*, 2014, pp. 6392–6399.

[15] C. D. Santina and A. Albu-Schäffer, "Exciting efficient oscillations in nonlinear mechanical systems through eigenmanifold stabilization," *IEEE Contr. Syst. Lett.*, early access, 2020, doi: 10.1109/LCSYS.2020.3048228.

[16] A. Albu-Schäffer and C. Della Santina, "A review on nonlinear modes in conservative mechanical systems," *Annu. Rev. Control*, vol. 50, pp. 49–71, 2020.

[17] K. J. Åström, "Oscillations in systems with relay feedback," *Adaptive Control, Filtering, and Signal Processing*. Berlin, Germany: Springer, 1995, pp. 1–25.

[18] C. Della Santina, D. Lakatos, A. Bicchi, and A. Albu-Schäffer, "Using nonlinear normal modes for execution of efficient cyclic motions in articulated soft robots," *Proc. Int. Symp. Exp. Robot.*, 2021.